Journal of Physics: Conference Series

PAPER • OPEN ACCESS

A multi-focusing contrast source Bayesian compressive method for solving inverse scattering problems

To cite this article: Giorgio Gottardi *et al* 2020 *J. Phys.: Conf. Ser.* **1476** 012013

A multi-focusing contrast source Bayesian compressive method for solving inverse scattering problems

Giorgio Gottardi, Mohammad Abdul Hannan, and Alessandro Polo

ELEDIA Research Center (ELEDIA@UniTN - University of Trento), Via Sommarive 9, I-38123 Trento, Italy

E-mail: giorgio.gottardi@unitn.it

Abstract. This work presents a novel inverse scattering (IS) methodology to deal with the retrieval of the electromagnetic (EM) properties of unknown scatterers. The proposed technique is based on the effective combination of a customized Bayesian compressive sensing (BCS) solver with the iterative multi-scaling approach ($IMSA$). Accordingly, *a-priori* information on the class of imaged targets as well as *progressively acquired* information on their location and size is exploited to yield accurate and robust reconstructions. Moreover, a contrast source inversion (CSI) formulation is adopted in order to enable the retrieval of non-Born scatterers. Numerical results are shown to verify the effectiveness of the proposed *IMSA-BCS-CSI* method, as well as to compare it with state-of-the-art alternatives.

1. Introduction

Non-invasively retrieving *qualitative* (i.e., location and shape) and *quantitative* (i.e., material composition) information on unknown targets starting from scattered field measurements requires to solve an inverse scattering (IS) problem. As it is well-known, such a problem is highly *non-linear* and *ill-posed* [1][2]. For such a reason, many techniques have been proposed to tackle these issues and yield robust and accurate reconstructions in many applicative scenarios including subsurface imaging [3]-[5], biomedical imaging [6][7], and non-destructive testing and evaluation [2]. Within this context, the Born approximation (BA) has been often invoked to restore the linearity of the IS problem [8]-[11]. However, its range of applicability is limited to weak scatterers or to scenarios in which the estimation of qualitative information is enough. Higher-order approximations (e.g., the second-order Born approximation, $SOBA$ [3]), Born iterative methods (BIMs), and distorted Born iterative methods ($DBIM$s [12]) have been explored, as well, to deal with the microwave imaging (MI) of stronger scatterers. Alternatively, the iterative multi-scaling approach ($IMSA$) proved to be a valid countermeasure to both *non-linearity* and *ill-posedness*, allowing to (i) reduce the ratio between unknowns and informative data, (ii) adaptively increase the resolution only within the regions of interest (RoIs), and (iii) exploit *progressively acquired* information on the imaged scenario in successive (higher-resolution) inversions [3][4][9].

Dealing with the *ill-posedness* of the IS problem, it is well-known that exploiting *a-priori* information on the class of imaged targets is an effective recipe to restore the solution stability in presence of noise [1]. Within this framework, compressive sensing (CS) methodologies [13]-[16] are effective regularizers, allowing to enforce *sparseness priors* with respect to a suitably-chosen representation (e.g., pixel [9], wavelet [15], total variation [8]). Moreover, those based on a

Bayesian formulation (BCS) [17] attracted articular attention since they do not require that the involved kernel operator satisfies the restricted isometry property (RIP) [13].
However, standard CS and BCS methods do not allow to exploit additional information besides that on the solution sparsity. To overcome such a limitation, this work presents an innovate *IS* method based on the effective integration of a customized BCS solver with the *IMSA*. Thanks to the exploitation of a constrained relevance vector machine (*C-RVM*), *progressively acquired* information through successive *IMSA* steps on the target location and size can be exploited to guide and improve the BCS solution. Moreover (as verified in Sect. 3) thanks to the formulation of the *IS* problem within a contrast source inversion (*CSI*) framework [18][19], the proposed method overcomes a state-of-the-art solution based on the BA [9], being able to accurately image non-Born targets, as well.

2. Mathematical Formulation

With reference to a $2D$ transverse magnetic (TM) *IS* scenario, let us consider an investigation domain $\mathcal{D}$ inside an homogeneous lossless medium having permittivity ε_0 and permeability μ_0. The presence of a target within $\mathcal{D}$ is mathematically described by means of the so-called *object function*

$$\tau(\mathbf{r}) = [\varepsilon_r(\mathbf{r}) - 1] - j\frac{\sigma(\mathbf{r})}{2\pi f\varepsilon_0} \tag{1}$$

where $\varepsilon_r(\mathbf{r})$ and $\sigma(\mathbf{r})$ are the relative permittivity and conductivity at position $\mathbf{r} \in \mathcal{D}$, respectively, f being the frequency, and $\mathbf{r} = (x, y)$. In order to retrieve an image of $\mathcal{D}$, a set of V z-polarized plane waves impinging from angular directions $\phi_v = [2\pi(v-1)/V]$, $v = 1, ..., V$, is exploited. Adopting a *CSI* formulation [18][19], the scattered field under the v-th illumination complies with the following *data* integral equation

$$E_s^v(\mathbf{r}) = [E^v(\mathbf{r}) - E_i^v(\mathbf{r})] = \int_{\mathcal{D}} \chi^v(\mathbf{r}') G(\mathbf{r}, \mathbf{r}') d\mathbf{r}'; \quad v = 1, ..., V \tag{2}$$

where $E_i^v(\mathbf{r})$ and $E^v(\mathbf{r})$ are the incident and total field, respectively, and $G(\mathbf{r}, \mathbf{r}')$ is the free-space Green's function. Moreover, $\chi^v(\mathbf{r})$ is the v-th *contrast source*, defined as

$$\chi^v(\mathbf{r}) = E^v(\mathbf{r})\tau(\mathbf{r}); \quad \mathbf{r} \in D;\ v = 1, ..., V. \tag{3}$$

Under these assumptions, the *IS* problem at hand is aimed at retrieving a guess of the object function inside $\mathcal{D}$ starting from the knowledge of $E_i^v(\mathbf{r})$, $v = 1, ..., V$, and of the corresponding scattered field samples collected by M ideal field probes located in $\mathbf{r}_m \in \Psi$, $m = 1, ..., M$, Ψ being an external observation domain not intersecting $\mathcal{D}$.
The solution of such a problem is found numerically by means of an hybrid inversion methodology based on the integration of a customized BCS solver with the *IMSA*. More in detail, the proposed *IMSA-BCS-CSI* method iteratively solves (2), updating at each s-th inversion step ($s = 1, ..., S$) the *RoI* $\mathcal{D}_s \subset \mathcal{D}_{s-1} \subset ... \subset \mathcal{D}_1 = \mathcal{D}$ and increasing the resolution within such a region for the successive reconstruction. Towards this end, the following multi-resolution representation of the unknown contrast sources is exploited at the s-th zooming stage

$$\chi_s^v(\mathbf{r}) = \sum_{t=1}^{s}\sum_{n=1}^{N_t} \chi_{t,n}^v \Phi_{t,n}(\mathbf{r}); \quad v = 1, ..., V \tag{4}$$

where N_t is the number of pixels at the t-th resolution level ($t = 1, ..., s$), while $\chi_{t,n}^v = \chi^v(\mathbf{r}_{t,n})$, $\mathbf{r}_{t,n}$ being the barycenter of the n-th pixel at the t-th resolution level (i.e., $\mathcal{D}_{t,n} \in \mathcal{D}_t$). Moreover, $\{\Phi_{t,n}(\mathbf{r});\ n = 1, ..., N_t;\ t = 1, ..., s\}$ are multi-resolution pixel basis functions defined as

$$\Phi_{t,n}(\mathbf{r}) = \left\{ \begin{array}{ll} 1 & \text{if } \mathbf{r} \in \mathcal{D}_{t,n} \text{ and } \mathbf{r} \notin \mathcal{D}_{t+1} \\ 0 & \text{otherwise} \end{array} \right. ; \quad n = 1, ..., N_t;\ t = 1, ..., s. \tag{5}$$

Accordingly, (2) is rewritten at the s-th inversion step in compact matrix notation as

$$\underline{E}^v = \underline{\underline{G}}_s \underline{\chi}_s^v \tag{6}$$

where $\underline{E}^v \in \mathbb{R}^{2M\times 1}$ contains the real/imaginary parts of the scattered field, $\underline{\chi}_s^v \in \mathbb{R}^{2L_s\times 1}$ contains the real/imaginary parts of the $L_s = \sum_{t=1}^{s} N_t$ unknown contrast source coefficients in (4), while $\underline{\underline{G}}_s \in \mathbb{R}^{2M\times 2L_s}$ is the corresponding multi-resolution Green's operator. According to the *BCS* theory, the solution of (6) is computed in closed form without the need to perform computationally-unaffordable checks of the *RIP* compliance by $\underline{\underline{G}}_s$ as follows

$$\hat{\underline{\chi}}_s^v = \frac{1}{\hat{\eta}_s^v}\left[\frac{\underline{\underline{G}}_s^T \underline{\underline{G}}_s}{\hat{\eta}_s^v} + \mathrm{diag}\left(\hat{\underline{a}}_s^v\right)\right]^{-1} \underline{\underline{G}}_s^T \underline{E}^v; \quad v = 1, ..., V \tag{7}$$

where $.^T$ is the transpose, while $\hat{\eta}_s^v$ and $\hat{\underline{a}}_s^v = \left\{\hat{a}_{s,l}^v;\, l = 1, ..., 2L_s\right\}$ are the *BCS* estimated noise variance and hyper-parameters, computed as

$$\left(\hat{\eta}_s^v, \hat{\underline{a}}_s^v\right) = \arg\left\{\max_{\left(\eta_s^v, \underline{a}_s^v\right)} \mathcal{L}\left(\underline{E}^v | \underline{\underline{G}}_s, \eta_s^v, \underline{a}_s^v\right)\right\} \tag{8}$$

where $\mathcal{L}\left(\underline{E}^v | \underline{\underline{G}}_s, \eta_s^v, \underline{a}_s^v\right)$ is the *BCS* logarithmic likelihood function [17][20]. It is worth observing that according to (7) each hyper-parameter directly influences the corresponding entry of $\underline{\chi}_s^v$. Accordingly, in order to exploit *progressively acquired* information on the solution from previous iterations, (8) is solved by means of a customized constrained relevance vector machine (*C-RVM*), enforcing that only the $2N_s < 2L_s$ entries of $\hat{\underline{a}}_s^v$ associated to pixels falling within the *RoI* at the s-th step are updated by the maximization procedure [1]. Once the contrast sources have been estimated through (7), the object function in each pixel is computed by averaging over different views ($v = 1, ..., V$) the ratio between retrieved currents and the corresponding total electric field. To summarize, the *IMSA-BCS-CSI* method consists in the following procedural steps

(i) *Low-Resolution (LR) Inversion.* Set $s = 1$ and partition the *RoI* $\mathcal{D}_1 = \mathcal{D}$ into N sub-domains. Solve the *LR* inverse problem (7)-(8), then compute the estimated *LR* object function.

(ii) *RoI Updating.* Set $s \leftarrow (s+1)$ then apply the *IMSA* filtering and clustering procedure [9] on the previous solution to update the *RoI* at the s-th step, $\mathcal{D}_s \subset \mathcal{D}_{s-1}$, by computing its barycenter $\mathbf{r}_s = (x_s, y_s)$ and its side L_s according to the procedure described in [9];

(iii) *High-Resolution (HR) Inversion.* Partition $\mathcal{D}_s$ into N sub-domains and solve the *HR* inverse problem (7)-(8) enforcing that only hyperparameters corresponding to pixels inside $\mathcal{D}_s$ are affected by the *C-RVM* search procedure. Finally, compute the estimated *HR* object function.

(iv) *Termination.* Stop if $s = S$ or if a stationary condition on the *RoI* size and location is met [9]. Otherwise, go to Step (ii).

[1] It is worth pointing out that all $(2L_s - 2N_s)$ remaining entries are forced to infinity by the *C-RVM*, such that corresponding entries of $\underline{\chi}_s^v$ are set to zero [20].

3. Numerical Results

This Section is aimed at numerically assessing the proposed *IMSA-BCS-CSI* methodology. Towards this end, some representative results are shown dealing with the imaging of a square investigation domain $\mathcal{D}$ of side 6λ, which has been probed by means of $V = 60$ incident plane waves. A set of $M = 60$ probes uniformly distributed over an external circular observation domain Ψ of radius $\rho = 4.5\lambda$ has been used to collect scattered data. Concerning the settings of the *IMSA-BCS-CSI*, $N = 100$ cells have been considered to discretize the *RoI* at each zooming step, the maximum number of *IMSA* steps being fixed to $S = 4$. To test the robustness of the method against noise, an additive white Gaussian noise has been superimposed on the scattered field, while the total integral error, defined as in [9], has been computed to give a quantitative measure of the obtained solution "quality".

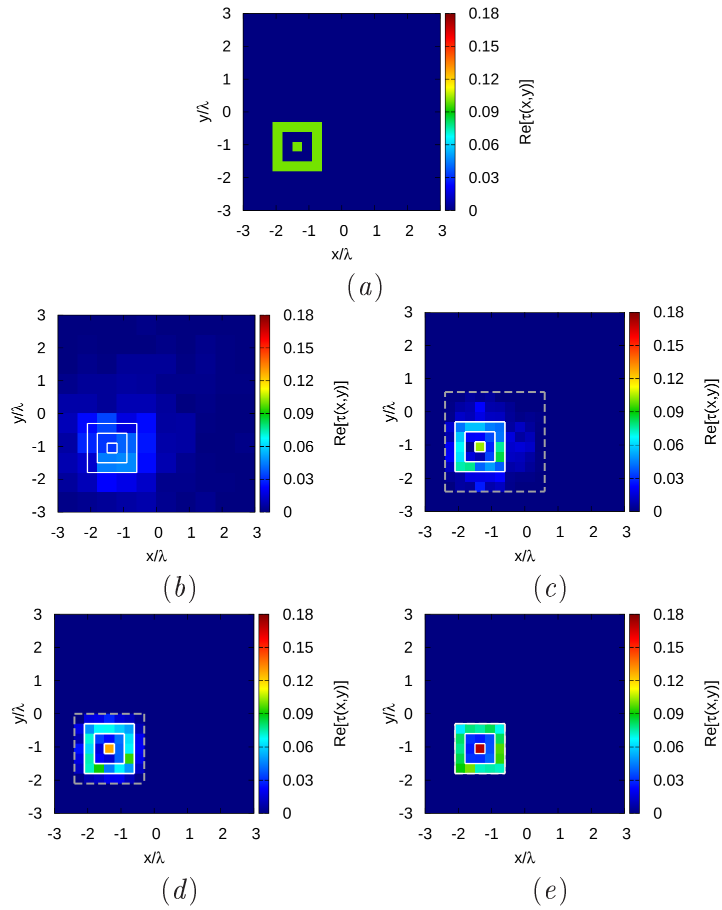

Figure 1. *Numerical Assessment* ("*Concentric Square*" Profile, $\tau = 0.1$, $SNR = 20$ dB) - (a) Actual and intermediate *IMSA-BCS-CSI* reconstructions at intermediate steps (b) $s = 1$, (c) $s = 2$, (d) $s = 3$, and (e) $s = S = 4$.

Figure 1 deals with the retrieval of the "*Concentric Square*" profile, whose actual dielectric profile is shown in Fig. 1(a) ($\tau = 0.1$ [2]). More in detail, the evolution of the *IMSA-BCS-CSI* solution through successive multi-scaling steps ($s = 1, ..., S$) has been reported when processing

[2] It should be pointed out that such a preliminary benchmark is aimed at assessing the effectiveness of the developed multi-scaling approach independently on the considered contrast value.

noisy data at $SNR = 20$ dB. As it can be observed, there is a progressive refinement of the reconstruction accuracy going from the LR inversion, in which the target location has been roughly detected [$s = 1$ - Fig. 1(b)], to the last HR step [$s = S = 4$ - Fig. 1(e)]. A dashed line has been plotted to indicate the extension of the RoI at each step. It can be inferred that the RoI has been progressively shrunk starting from $\mathcal{D}_1 = \mathcal{D}$ [Fig. 1(b)], perfectly matching the target support at the end of the multi-scaling process [Fig. 1(e)]. Moreover, thanks to the exploitation of the C-RVM solver, *progressively acquired* information on the target location and size has been successfully exploited, allowing to remove artifacts in the background and to achieve a faithful estimation of the object function [Fig. 1(e) vs. Fig. 1(a)]. For completeness, the actual and retrieved imaginary part of the contrast function at the last step have been reported in Fig. 2, confirming the accuracy of the developed approach.

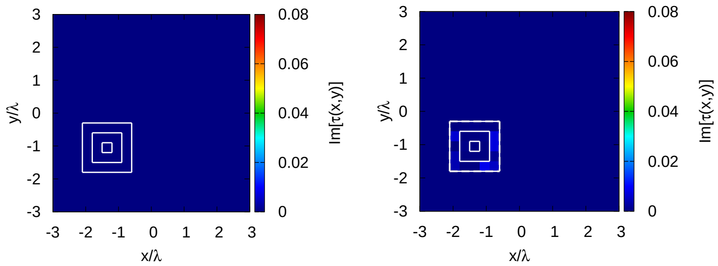

(a) (b)

Figure 2. *Numerical Assessment* ("*Concentric Square*" Profile, $\tau = 0.1$, $SNR = 20$ dB) - (a) Actual and (b) *IMSA-BCS-CSI* reconstruction ($s = S = 4$) of the imaginary part of the contrast function.

To further prove the effectiveness and robustness of the proposed method, Figure 3(b) shows the *IMSA-BCS-CSI* outcome when dealing with the retrieval of the "*Inhomogeneous Square*" profile [Fig. 3(a)], having a maximum object function equal to $\tau_{\max} = 0.6$, and processing highly-blurred data ($SNR = 5$ dB). As it can be seen, the target location and size have been correctly identified, with a good estimation of the object function [Fig. 3(b) vs. Fig. 3(a)], regardless of the very harsh imaging conditions. Even more interestingly, there is a clear advantage of the *IMSA-BCS-CSI* over a state-of-the-art multi-scaling BCS method based on the first order Born approximation (*IMSA-BCS-BA* [9]). Indeed, the plot in Fig. 3(c), showing the *IMSA-BCS-BA* result for the same test case, indicates that such method is only able to detect the presence of the target and to roughly estimate its location, being however incapable of correctly detecting its actual support and object function.
To complete the comparative assessment, the result yielded by the *BARE-BCS-CSI* method, based on a standard *non-iterative single-resolution BCS* solver working in the *CSI* framework, has been reported in Fig. 3(d) ($N = 400$). Although the *CSI* formulation allowed to detect the presence of the inner core of the target with higher contrast, overall the reconstruction quality is significantly lower with respect to the *IMSA* method, with many artifacts arising in the background region, as well [Fig. 3(b) vs. Fig. 3(d)]. Quantitatively, the behavior of the total reconstruction error has been reported in Fig. 4 as a function of $\tau_{\max}$ for both *IMSA-BCS-CSI* and *BARE-BCS-CSI*, confirming the superior performance of the proposed method whatever the level of noise and the actual contrast.

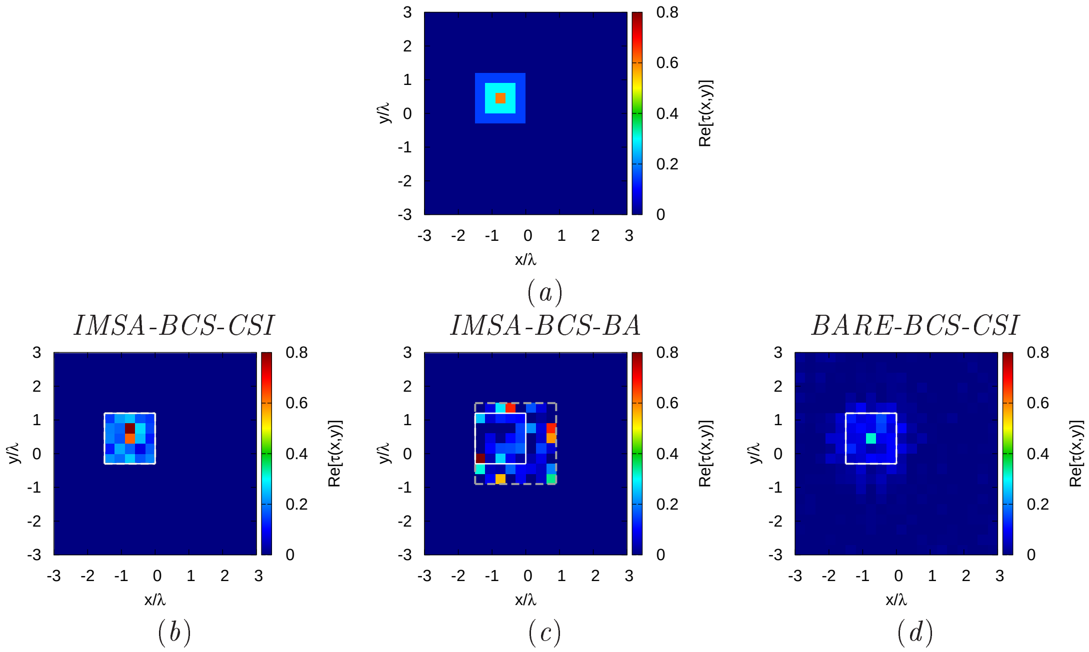

Figure 3. *Numerical Assessment* ("*Inhomogeneous Square*" Profile, $\tau_{\max} = 0.6$, $SNR = 5$ dB) - (a) Actual and retrieved contrast distribution by the (b) *IMSA-BCS-CSI*, (c) *IMSA-BCS-BA*, and (d) *BARE-BCS-CSI* methods.

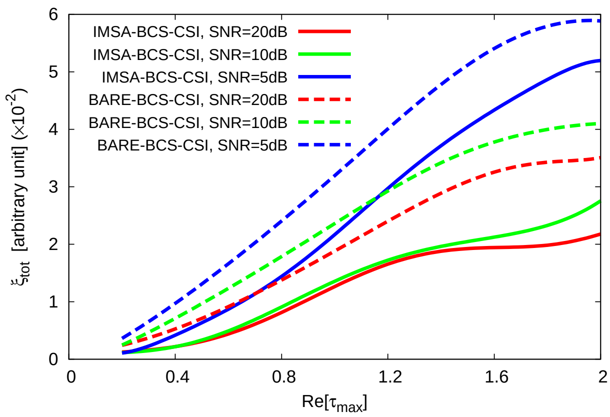

Figure 4. *Numerical Assessment* ("*Inhomogeneous Square*" Profile, $SNR \in [5, 20]$ dB) - Behavior of the total reconstruction error as a function of $\tau_{\max}$ for the *IMSA-BCS-CSI* and *BARE-BCS-CSI* methods.

4. Conclusions

This work presented an innovative *IS* method able to jointly exploit *a-priori* information on the class of imaged targets and *progressively acquired* information of their position and size. More in detail, *sparseness* priors have been exploited to regularize the solution thanks to a probabilistic formulation of the *IS* problem within the *CSI* framework. Furthermore, the integration of the

BCS solver with the *IMSA*, enabled thanks to the exploitation of a *C-RVM* solver, allowed to adaptively increase the resolution within the *RoI* and yield significant improvements in terms of reconstruction accuracy. Numerical results verified the effectiveness of the *IMSA-BCS-CSI* method, as well as its superior performance with respect to state-of-the-art alternatives.

Acknowledgments
This work benefited from the networking activities carried out within the SNATCH Project (2017-2019) funded by the Italian Ministry of Foreign Affairs and International Cooperation, Directorate General for Cultural and Economic Promotion and Innovation, and the Project "CYBER-PHYSICAL ELECTROMAGNETIC VISION: Context-Aware Electromagnetic Sensing and Smart Reaction (EMvisioning)" funded by the Italian Ministry of Education, University, and Research within the PRIN2017 Program.

References
[1] Chen X 2018 *Computational Methods for Electromagnetic Inverse Scattering* (Singapore: Wiley-IEEE)
[2] Zoughi R 2000 *Microwave Nondestructive Testing and Evaluation* (Amsterdam, The Netherlands: Kluwer)
[3] Salucci M, Oliveri G, Randazzo A, Pastorino M and Massa A 2014 Electromagnetic subsurface prospecting by a multi-focusing inexact Newton method within the second-order Born approximation *J. Opt. Soc. Am. A* **31** 1167-1179
[4] Salucci M, Poli L and Massa A 2017 Advanced multi-frequency GPR data processing for non-linear deterministic imaging *Signal Proc.* **132** 306-318
[5] Salucci M, Gelmini A, Poli L, Oliveri G and Massa A 2018 Progressive compressive sensing for exploiting frequency-diversity in *GPR* imaging *J. Electromagn. Waves Appl.* **32** 1164-1193
[6] Zamani A, Abbosh A M and Crozier S 2017 Multistatic biomedical microwave imaging using spatial interpolator for extended virtual antenna array *IEEE Trans. Antennas Propag.* **65** 1121-1130
[7] Salucci M, Gelmini A, Vrba J, Merunka I, Oliveri G and Rocca P 2019 Instantaneous brain stroke classification and localization from real scattering data Microw. Opt. Technol. Lett. **61** 805-808
[8] Oliveri G, Anselmi N and Massa A 2014 Compressive sensing imaging of non-sparse 2D scatterers by a total-variation approach within the Born approximation *IEEE Trans. Antennas Propag.* **62** 5157-5170
[9] Anselmi N, Poli L, Oliveri G and Massa A 2018 Iterative multi-resolution bayesian CS for microwave imaging *IEEE Trans. Antennas Propag.* **66** 3665-3677
[10] Slaney M, Kak AC and Larsen LE 1984 Limitations of imaging with first-order diffraction tomography *IEEE Trans. Microw. Theory Techn.* **32** 860-874
[11] Shumakov D and Nikolova N 2018 Fast quantitative microwave imaging with scattered-power maps *IEEE Trans. Microw. Theory Techn.* **66** 439-449
[12] Gilmore C, Mojabi P and LoVetri J 2009 Comparison of an enhanced distorted Born iterative method and the multiplicative-regularized contrast source inversion method *IEEE Trans. Antennas Propag.* **57** 2341-2351
[13] Oliveri G, Salucci M, Anselmi N and Massa A 2017 Compressive sensing as applied to inverse problems for imaging: theory, applications, current trends, and open challenges *IEEE Antennas Propag. Mag.* **59** 34-46
[14] Li S, Zhao G, Sun H and Amin M 2018 Compressive sensing imaging of 3-D object by a holographic algorithm *IEEE Trans. Antennas Propag.* **66** 7295-7304
[15] Anselmi N, Oliveri G, Hannan M A, Salucci M and Massa A 2017 Color compressive sensing imaging of arbitrary-shaped scatterers *IEEE Trans. Microwave Theory Techn.* **65** 1986-1999
[16] Winters D W, Van Veen B D and Hagness S C 2010 A sparsity regularization approach to the electromagnetic inverse scattering problem *IEEE Trans. Antennas Propag.* **58** 145-154
[17] Ji S, Xue Y and Carin L 2008 Bayesian compressive sensing *IEEE Trans. Sig. Proc.* **56** 2346-2356
[18] Li M, Abubakar A and Van Den Berg P M 2009 Application of the multiplicative regularized contrast source inversion method on 3D experimental Fresnel data *Inverse Probl.* **25** 1-23
[19] Van den Berg P M and Abubakar A 2001 Contrast source inversion method: State of art *Progress In Electromagnetics Research* **34** 189-218
[20] Tipping ME 2001 Sparse Bayesian learning and the relevant vector machine *J. Mach. Learn. Res.* **1** 211-244